Crystallization induced by multiple seeds: Dynamical density functional approach

T. Neuhaus,[1] M. Schmiedeberg,[1,2,*] and H. Löwen[1,†]

[1]*Institut für Theoretische Physik II: Weiche Materie, Heinrich-Heine-Universität Düsseldorf, Universitätsstraße 1, D-40225 Düsseldorf, Germany*

[2]*Fachbereich Physik, Universität Osnabrück, D-49076 Osnabrück, Germany*

(Received 24 September 2013; published 30 December 2013)

Using microscopic dynamical density functional theory, we calculate the dynamical formation of polycrystals by following the crystal growth around multiple crystalline seeds imposed to an undercooled fluid. Depending on the undercooling and the size ratio as well as the relative crystal orientation of two neighboring seeds, three possibilities of the final state emerge, namely no crystallization at all, formation of a monocrystal, or two crystallites separated by a curved grain boundary. Our results, which are obtained for two-dimensional hard disk systems using a fundamental-measure density functional, shed new light on the particle-resolved structure and growth of polycrystalline material in general.

DOI: 10.1103/PhysRevE.88.062316 PACS number(s): 64.70.D−, 82.70.Dd, 05.20.Jj

I. INTRODUCTION

Our quantitative understanding of crystallization processes out of an undercooled melt dates back to the classical papers by Kolmogorov [1], Johnson and Mehl [2], and Avrami [3], for reviews see [4,5]. The underlying picture is that critical nuclei are formed which are randomly distributed in space and time. These nuclei then act as seeds for further crystal growth. The emerging crystallites grow independently from each other until they meet and form a grain boundary resulting in a polycrystalline texture of different crystallites with different orientations (see, e.g., [6–8]).

Experiments on colloids [6,9–11] and complex plasmas [12] allow a determination of the resulting grain boundaries on the particle scale [13,14] and have largely increased our information about the microscopic processes underlying crystallization in two and three spatial dimensions, often supplemented by particle-resolved computer simulations [15]. However, as far as a microscopic theory is concerned, much less has been done. Such a theory describing crystallization is nontrivial since it requires a unifying description of both the melt and the solid phase. Classical density functional theory (DFT) of inhomogeneous liquids [16–18] provides such an approach which can even be generalized towards Brownian dynamics appropriate for colloids [19–21] such that DFT is an ideal tool for crystallization [22]. DFT needs an accurate equilibrium free energy density functional as an input. Recently developed fundamental measure theory provides accurate functionals for hard spheres [23] and hard disks [24]. DFT can be coarse grained to obtain a more approximative phase-field-crystal (PFC) model [25,26], which has been extensively used to explore crystallization process around imposed seeds, see, e.g., Refs. [27–29].

One of the key stages of crystallization is when two growing crystallites meet and merge forming a grain boundary. This is most cleanly seen in a setup of two single neighboring small crystal seeds which are misoriented relative to each other such that a grain boundary is likely to emerge and to persist. Such a setup with two seeds has never been studied in previous DFT calculations although crystal growth around a single prescribed crystalline seed is the standard starting configuration for most of the calculations [30,31] and grain boundaries have been largely generated by other setups or by PFC approaches [32–39].

In this paper we close this gap and study systematically a two-dimensional situation of two neighboring seeds around which different crystallites grow until they meet forming a grain boundary. We employ microscopic dynamical density functional theory (DDFT) by using the fundamental-measure theory for hard disks [24] to calculate the formation of polycrystalline domains. Depending on the undercooling (or overcompression), the size ratio, and the relative crystal orientation of the two neighboring seeds, three possibilities of the final state emerge: (i) no crystallization at all, (ii) formation of a monocrystal, and (iii) two crystallites separated by a curved grain boundary. Finally, we also consider three seeds forming various grain boundaries. Our results shed new light on the particle-resolved structure and growth of polycrystalline material in general.

Our prediction can directly be verified in particle-resolved experiments on colloidal suspensions [10,14]. Any setup for an initial crystalline seed can be realized by fixing an arbitrary number of individual particles to prescribed positions within a solution of other particles, see [40] for an example of two-dimensional colloids. As the dynamics of the colloids is Brownian, which exactly matches the conditions of our DDFT, a precise design of our setup is possible.

This article is organized as follows: We introduce the underlying setup in the following Sec. II and continue with a brief introduction to dynamical density functional theory in Sec. III. We then explore the long-time limit of two crystallites in Sec. IV as well as the dynamics of the observed grain boundaries in Sec. V. After this, we focus on the interplay of three nuclei in Sec. VI and finally, we conclude our results in Sec. VII.

II. THE SETUP

In our model systems, two crystalline nuclei containing N_i $(i = 1,2)$ hard disks with diameter σ are placed on a

*schmiedeberg@thphy.uni-duesseldorf.de
†hlowen@thphy.uni-duesseldorf.de

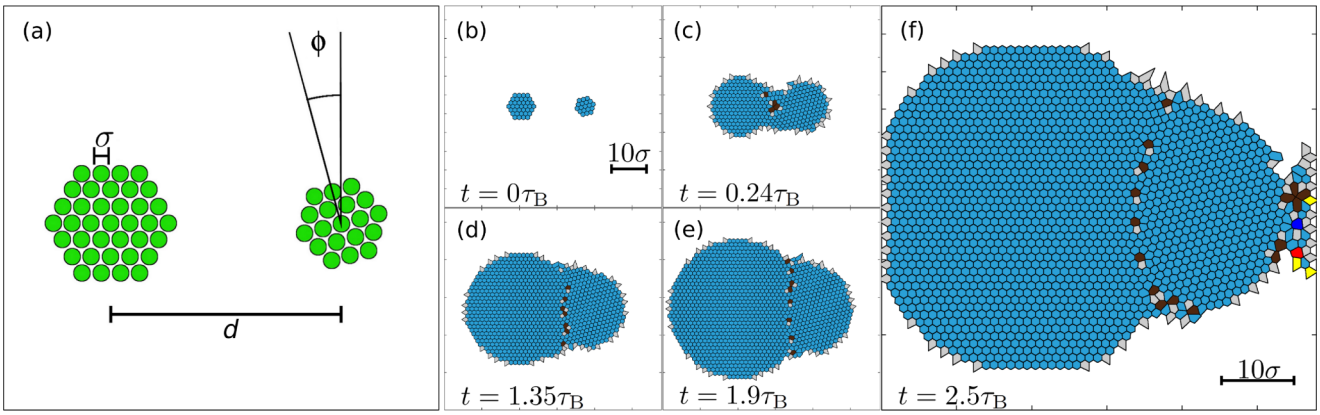

FIG. 1. (Color online) (a) Schematic view of the initial nuclei of hard spheres with diameter σ separated by a distance d and surrounded by a homogeneous fluid, at area fraction η. Here the left nucleus consists of $N_1 = 61$ particles, whereas the right nucleus is built of $N_2 = 37$ particles and additionally rotated by an angle ϕ. (b)–(f) The Voronoi construction of an exemplary growth at times $t = 0, 0.24, 1.35, 1.9, 2.5\tau_B$, where blue (medium gray) cells have six neighboring particles and defects with more or less neighboring particles are coded in different colors (light or dark gray) all surrounded by a fluid. A grain boundary grows, first on a straight and finally on a curved line between the two crystalline regions. For a movie of the growth see Supplemental Material [41].

flat substrate. In Fig. 1(a) a schematic view of the nuclei is displayed. Here the left nucleus consists of $N_1 = 61$ and the right of $N_2 = 37$ particles. Note that both seeds as well as all seeds that will be employed later in this article are larger than the critical nuclei that is needed for crystallization. Both possess hexagonal symmetry and exhibit at center-to-center distance d. The right nucleus is rotated counterclockwise by an angle ϕ. Furthermore, the nuclei are surrounded by a homogeneous fluid such that the area fraction η of the system remains constant. We employ periodic boundary conditions with a simulation box that is chosen large enough such that its boundaries are only reached late in the simulations. An exemplary growth process is depicted in Figs. 1(b)–1(f) as well as a movie in Supplemental Material [41]. Blue (medium gray) colored Voronoi cells show crystalline regions with six nearest neighbors in contrast to cells with any other number of neighbors that are depicted with other colors (light and dark gray). When the interfaces of the growing crystals coincide, defects are caused by the incompatibility of the two crystal lattices. Depending on the initial configuration, these defects vanish or remain stable. In the case shown in Fig. 1, a stable grain boundary is obtained. During the growth process, it shifts towards the smaller nucleus and additionally tilts around it resulting in a curved grain boundary. Radii of curvature will be extracted later in this article for different distances d and size ratios N_1/N_2. Furthermore, the occurrence of a grain boundary is systematically studied depending on size ratio, area fraction η, and angle of rotation ϕ.

III. DYNAMICAL DENSITY FUNCTIONAL THEORY

In order to calculate the dynamics of crystal growth, we use DDFT which is based on classical DFT [16,23,42–44] but recovers the motion of Brownian particles. It can be derived from the exact Smoluchowski equation [19–21] invoking an adiabatic approximation. The density profile $\rho(\mathbf{r},t)$ consequently depends on time and it is given by a generalized diffusion equation

$$\frac{\partial\rho(\mathbf{r},t)}{\partial t} = (k_B T)^{-1} D\nabla\cdot\left(\rho(\mathbf{r},t)\nabla\frac{\delta\Omega[T,A,\mu,\rho(\mathbf{r},t)]}{\delta\rho(\mathbf{r},t)}\right). \tag{1}$$

Here D indicates the short-time diffusion coefficient and k_B is Boltzmann's constant. DDFT is based on the knowledge of the equilibrium grand canonical free energy $\Omega\{T,A,\mu,[\rho(\mathbf{r},t)]\}$ which depends on temperature T, the accessible area A, the chemical potential μ, and which is a functional of the time-dependent density profile $\rho(\mathbf{r},t)$. The chemical potential μ is used as a Lagrangian multiplier in order to fix the average particle number inside the system which will be defined via the bulk area fraction η. $\Omega[\rho(\mathbf{r},t)]$ can be split into three terms: A first contribution given by an ideal gas $\mathcal{F}_{\rm id}[\rho(\mathbf{r})] = k_B T\int d\mathbf{r}\rho(\mathbf{r})\{\ln[\Lambda^2\rho(\mathbf{r})] - 1\}$ which contains the (irrelevant) thermal wavelength Λ, a second term resulting from the interactions with an external potential $\mathcal{F}_{\rm ext}[\rho(\mathbf{r})] = \int d\mathbf{r}\rho(\mathbf{r})[V_{\rm ext}(\mathbf{r}) - \mu]$, and a third term which describes the interactions of particles $\mathcal{F}_{\rm exc}[\rho(\mathbf{r})]$, called the excess free energy. For the latter we use [24] a recently developed fundamental measure approach for hard disks.

The initial nuclei are created by exposing an external pinning potential with Gaussian shape at the intended particle positions $\mathbf{r}_i$ to a homogeneous fluid. This potential reads

$$V_{\rm p}(\mathbf{r}) = \sum_i V_{\rm p}^{(0)} e^{-\alpha(\mathbf{r}-\mathbf{r}_i)^2}, \tag{2}$$

containing a width $\alpha\sigma^2 = 6$ and a strong amplitude $V_{\rm p}^{(0)}/k_B T = 4$. After a short time of $t = 0.07\tau_B$, where $\tau_B = \sigma^2/D$ is the Brownian time, the nuclei are grown and the pinning potential is switched off [31]. Then, the crystal grows and the growth dynamics of multiple seeds can be examined.

Note that DFT or DDFT does not contain noise (thermal fluctuations) or capillary waves that might influence crystal growth in particular concerning the shape of the critical

crystalline nucleus [45]. Here we consider the growth of an almost flat crystalline-fluid interface where capillary waves enlarge the interfacial width but do not destroy the growth mechanism. In fact, recent comparisons of DFT calculations and simulations on surface tension suggest that the predictions obtained by DFT are in reasonable agreement with the results obtained from simulations [46,47].

IV. LONG-TIME LIMIT

In the following, the long-time limit of crystal growth will be examined. At a distance $d = 10\sigma$, two nuclei are positioned and the right nucleus is rotated by ϕ. Depending on the seed sizes N_1 and N_2, the prescribed bulk area fraction η, and the rotation angle ϕ, three different types of behavior can be observed in the long-time limit. First, a homogeneous metastable fluid phase can occur at low area fractions [see Fig. 2(a)]. Due to the interaction of the two crystalline regions, both crystals melt resulting in a fluid. At small rotation angles but intermediate area fractions, the resulting phase is a monocrystal as exemplary shown in Fig. 2(b). When the crystal-fluid interfaces of the two crystals reach each other, particles rearrange such that one crystalline region adapts the orientation of the other. Hence, this crystal grows unperturbed and fills the whole simulation box. If the rotation angle is sufficiently large, two crystalline regions are observed separated by a grain boundary [see Fig. 2(c)]. In this case, the particles stay at their positions such that the two crystals do not rearrange. The shape of the grain boundary depends on the initial configuration. For two equally sized nuclei, as shown in Fig. 2(c), the resulting grain boundary is a straight line. In Fig. 2(c) the line is slightly tilted at the upper and lower edge of the box resulting from periodic boundary conditions. Note that in case of seeds with different sizes, the resulting grain boundary usually moves in the direction of the smaller seed as we will discuss in the next section. For the diagrams in Fig. 2 we only determined whether the grain boundary disappears or prevails. Defects in the grain boundary consist of pairs of particles, such that one particle has seven neighbors and the other particle has only five neighbors.

The exact phase behavior additionally depends on the size ratio of the initial nuclei N_1/N_2. In the case of both nuclei being of the same size; $N_1 = N_2 = 19$ as shown in Fig. 2(d); a fluid phase illustrated by blue triangles is observed which is not seen for differently sized nuclei in the examined regime of area fractions. In case of $N_1 = 61$ and $N_2 = 37$, as shown in Fig. 2(e), the boundary between the monocrystalline phase and the phase with grain boundary shifts towards smaller area fractions, as the crystals have strongly peaked density distributions. Hence, lower area fractions are sufficient for the smaller nucleus to remain stable. If both nuclei are smaller ($N_1 = 37$ and $N_2 = 19$), the phase boundary is strongly shifted to higher area fractions. In this case, at low area fractions the bigger nucleus forms a more stable crystal—with larger density peaks—which modifies the smaller crystal such that it finally fills the entire simulation box and no grain boundary or melting is observed. The latter case is visualized in Fig. 2(f). At large area fractions and large rotation angles, the grain boundary remains stable in all cases, while at small rotation

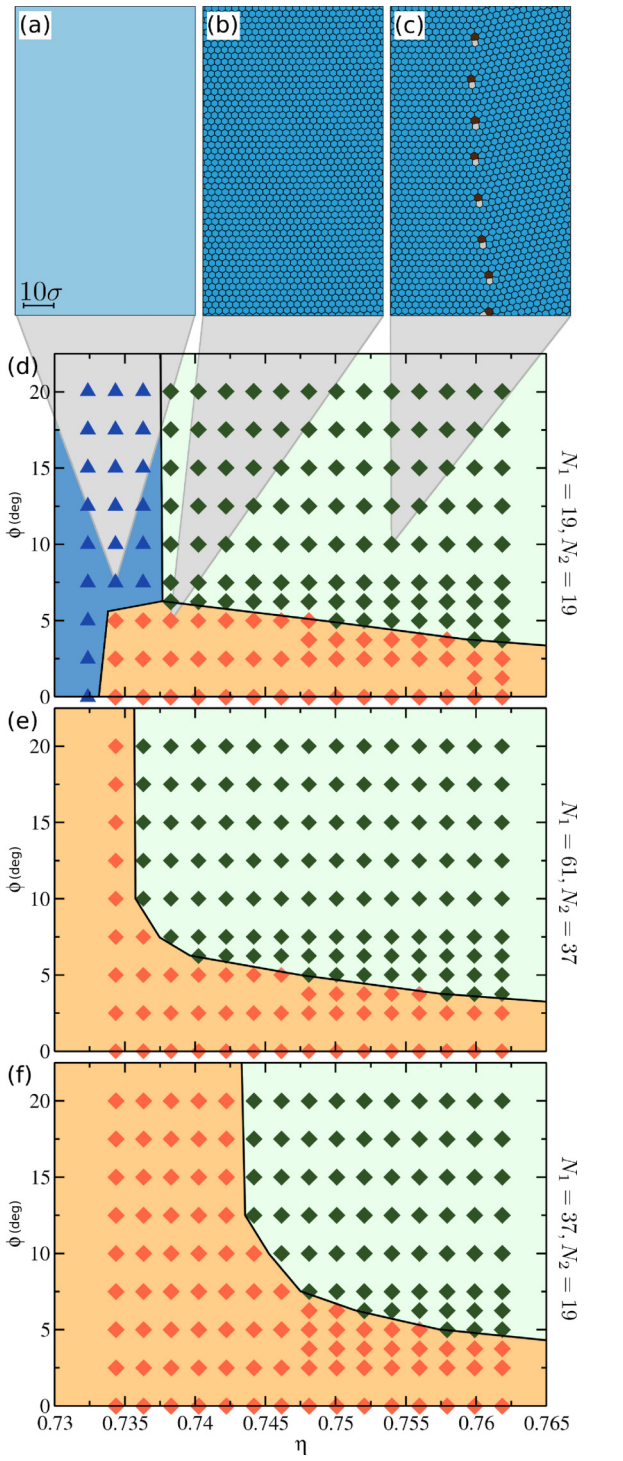

FIG. 2. (Color online) Long-time situations of the interaction of two nuclei at distance $d = 10\sigma$ rotated with respect to each other by an angle ϕ at area fraction η. The resulting cases are (a) a fluid, (b) a monocrystal, and (c) a crystal with a grain boundary where only cutouts of the full quadratic simulation box are shown. (d)–(f) The phase diagrams for different nuclei sizes where blue triangles indicate a fluid, red (gray) diamonds denote a monocrystal, and dark green (dark gray) diamonds label the crystalline region with a stable grain boundary. The nuclei consist of (d) $N_1 = N_2 = 19$, (e) $N_1 = 61$, $N_2 = 37$, and (f) $N_1 = 37$, $N_2 = 19$ particles. For movies of the situations (a)–(c) as well as a movie for $N_1 = N_2 = 19$, $\phi = 5^\circ$, and $\eta = 0.754$, see Supplemental Material [41].

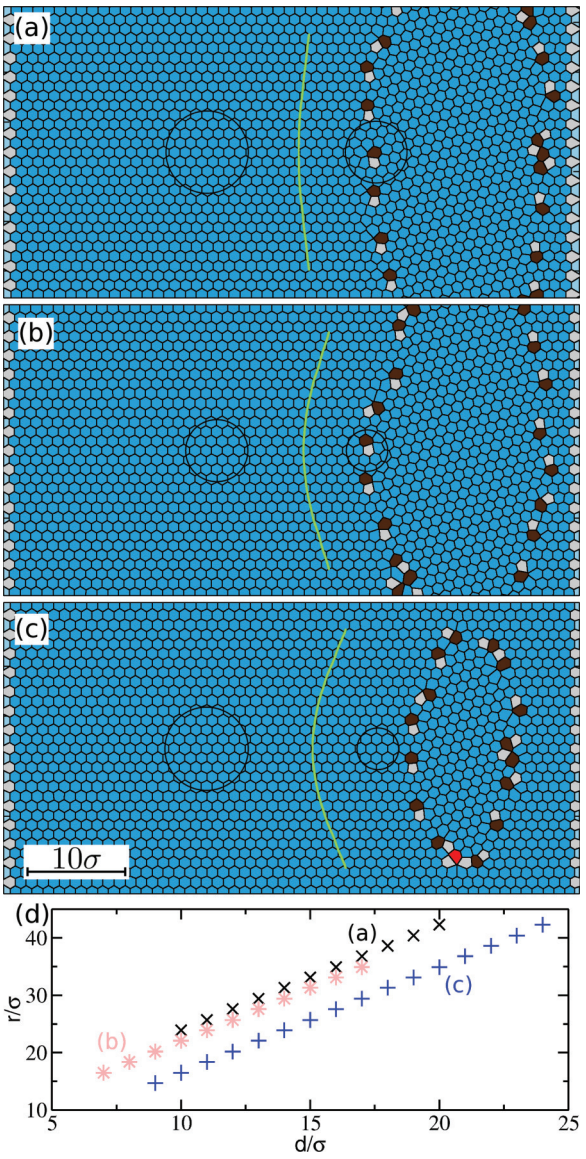

FIG. 3. (Color online) Analysis of the grain boundaries between two grown crystalline regions after a time $t = 4\tau_B$, where the initial right nucleus is rotated by $\phi = 20^\circ$ for different nuclei sizes: (a) $N_1 = 61$, $N_2 = 37$, (b) $N_1 = 37$, $N_2 = 19$, and (c) $N_1 = 61$, $N_2 = 19$. The area fractions are chosen such that grain boundaries occur. The shown Voronoi cells are colored in dark blue (medium gray) for six neighbors in contrast to defects depicted with other colors (light or dark gray). Black circles indicate the spherically modeled initial nuclei and the green (light gray) line displays the analytically calculated interface. (d) The extracted radii of curvature for cases (a)–(c) obtained at different distances d between the initial nuclei. For movies of the growth, see Supplemental Material [41].

angles the adaption is minimal enough such that there is a monocrystalline phase for any area fraction we examined.

V. DYNAMICS OF GRAIN BOUNDARIES

With the knowledge of the long-time limit, now the dynamics of the grain boundary will be focused on. Again, two nuclei are positioned at various distances d but at a fixed

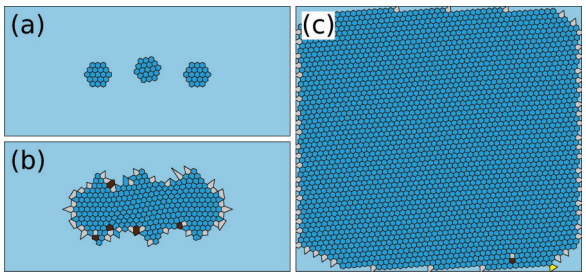

FIG. 4. (Color online) Time series of the crystal growth dynamics originated from three nuclei of 19 particles. Shown is a Voronoi constructon of (a) the initial, (b) an intermediate ($t = 0.3\tau_B$), and (c) the configuration at $t = 4\tau_B$. The outer nuclei are positioned symmetrically around the center nucleus at distances $d = 10\sigma$, while the center nucleus is displaced vertically by 1σ. In addition, the latter is rotated by $\phi = 5^\circ$.

rotation angle $\phi = 20^\circ$. The area fraction of the system is chosen such that two crystalline regions separated by a grain boundary are obtained.

First, we determined the interface that one would expect from an unperturbed growth [green (light gray) lines in Figs. 3(a)–3(c)]. In order to obtain these lines, we determine the growth of a single nucleus with size N_1 or N_2 separately, and extract the distance the crystal has grown depending on time. In a next step, the nucleus is approximated by a sphere with a corresponding diameter and a geometric construction is performed in order to obtain the positions where the crystal-fluid interfaces of the two nuclei reach each other. Therefore, the green line correspond to the boundaries where the two crystals if grown unperturbed would first touch.

Second, we performed DDFT calculations of the corresponding growth processes. After the two growing crystals reach each other, a grain boundary develops that moves towards the smaller nucleus. Additionally, the radius of curvature r is smaller compared with the geometric construction. These observations are independent of the system size.

For longer times, a second grain boundary on the right develops that is the result from periodic boundary conditions used in our DDFT calculations. In principle this long-time behavior can be seen as a growth process that is started with an array of seeds. Figures 3(a)–3(c) show the configurations obtained by DDFT after a time $t = 4\tau_B$. The motion of the grain boundaries was slowed down due to the periodic boundary conditions. The radius of curvature can be extracted and is plotted as a function of distance d in Fig. 3(d). We

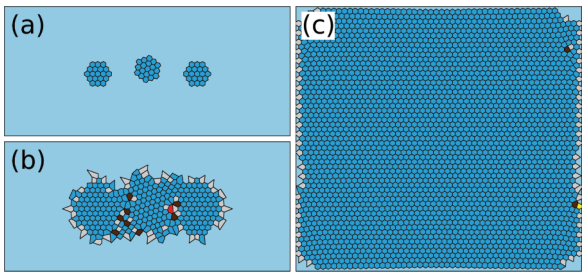

FIG. 5. (Color online) Similar to Fig. 4 but for a rotation angle $\phi = 20^\circ$.

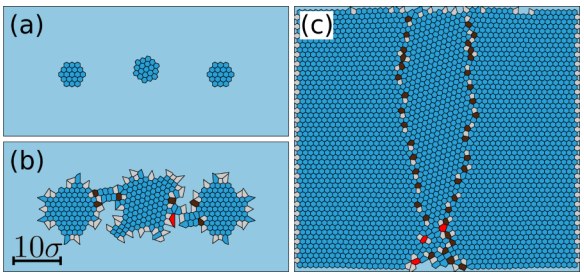

FIG. 6. (Color online) Similar to Fig. 4 but with distance $d = 15\sigma$ between the center and the outer nuclei.

compute three different size ratios N_1/N_2 [Figs. 3(b) and 3(c)] and the corresponding radii of curvature at distance d for all three cases. Due to the dependence on the system size caused by the periodic boundary conditions and due to further uncertainties when the radius is extracted through very few points, we only give a qualitative statement: With increasing distances, the radii also increase or in other words, the grain boundaries are closer to a straight line which is in agreement with the geometric construction. The further apart two nuclei are displaced, the less is the effect of the local curvature of each nucleus.

VI. THREE CRYSTAL NUCLEI

More than two nuclei can be studied as exemplary shown in Figs. 4, 5, and 6. Interestingly, very different final states can be obtained by employing different starting configurations. Especially, it is not obvious which crystal wins for the cases where the growth ends up in a monocrystal. In our example, the center nucleus is positioned symmetrically at distance d between two similar nuclei all with 19 particles, shifted upwards by 1σ and rotated by an angle ϕ. We observe three different configurations after a time $t = 4\tau_B$ depending on the initial conditions. In the case of a smaller distance $d = 10\sigma$ and small rotation angle $\phi = 5^\circ$ (Fig. 4), the resulting monocrystal adapts the orientation of the center nucleus. During the growth, the particles of the outer crystalline regions rearrange such that the center crystal grows. For a movie of this growth process, see Supplemental Material [41]. If this center nucleus is rotated more ($\phi = 15^\circ$), the orientation of the resulting monocrystal follows that of the outer nuclei as it can be seen in Fig. 5. By increasing the distance between the nuclei to $d = 15\sigma$, a third case can be observed and visualized in Fig. 6. Here we see two crystalline regions of different orientation—in analogy to the initial configuration—separated by a grain boundary. As the time each nucleus has to grow is larger because of a larger distance, the resulting crystalline regions are much more pronounced or in other words, the density distributions are stronger located. Consequently, none of the two crystals rearranges and stable grain boundaries are observed.

VII. CONCLUSIONS

In this paper we have shown that DDFT is a suitable tool to study crystal growth of hard disks on a microscopic scale. There are three different cases when two nuclei with incommensurate orientation grow—a fluid, a monocrystal, and a crystal with a stable grain boundary. We have studied the occurrence of these situations systematically depending on area fraction and angle of rotation. In addition, we examined the dynamics of the grain boundary while the two crystals grow for different distances and size ratios of the nuclei. The upper and lower end of the grain boundary tilts towards the smaller nucleus. From this tilted boundary, we have extracted the radii of curvature and compared the results with the geometric construction of an unperturbed growth. In this ideal model, the grain boundary results from the positions where growth interfaces of two nuclei meet. Since the larger nucleus dominates the growth process, the grain boundary obtained with DDFT is shifted towards the smaller nucleus compared with the geometric construction. Of course, even more nuclei can be positioned with even random size or orientation and the growth process can be studied.

Future work should concentrate on the following directions: First, an array of seeds would be interesting to explore in order to systematically study different distributions of seeds in space. Second, the rotation or shrinking dynamics of circular grains as observed with PFC models in [35,37,38] can also be studied using DFT. Third, DFT provides an ideal framework for crystallization in static external potentials such as gravity [48] that further studies should consider, e.g., crystallites growing in sedimentation [49]. Other interactions like soft spheres and attractions can be explored using for example the fundamental measure density functional for the Asakura-Oosawa model [50,51]. Moreover, the influence of shear on crystallization [6,52] and the resulting grain boundaries would be an interesting playground to apply our calculation to. Finally, a global arrangement of grain boundaries as induced by fluctuations over free energy barriers which are not contained in our density-functional theory needs to be looked at using more refined approaches which go beyond the mean-field approach.

ACKNOWLEDGMENTS

We thank M. Oettel for helpful discussions. This work was supported by the DFG via SPP 1296. M.S. also acknowledges support by the DFG within the Emmy-Noether program.

[1] A. N. Kolmogorov, Izv. Akad. Nauk. SSSR, Ser. Fiz. [Bull. Acad. Sci. USSR, Phys. Ser.] **1**, 355 (1937).
[2] W. A. Johnson and R. F. Mehl, Trans. Am. Inst. Min. Metall. Eng. **135**, 416 (1939).
[3] M. Avrami, J. Chem. Phys. **9**, 177 (1941).
[4] M. Fanfoni and M. Tomellini, Il Nuovo Cimento D **20**, 1171 (1998).
[5] M. C. Weinberg, D. P. Birnie, III, and V. A. Shneidman, J. Non-Cryst. Solids **219**, 89 (1997).
[6] T. Palberg, W. Monch, J. Schwarz, and P. Leiderer, J. Chem. Phys. **102**, 5082 (1995).
[7] D. C. Sayle, B. C. Mangili, D. W. Price, and T. X. Sayle, Phys. Chem. Chem. Phys. **12**, 8584 (2010).

[8] S. Forest, F. Barbe, and G. Cailletaud, Int. J. Solids Struct. **37**, 7105 (2000).
[9] T. Palberg, J. Phys.: Condens. Matter **11**, R323 (1999).
[10] A. M. Alsayed, M. F. Islam, J. Zhang, P. J. Collings, and A. G. Yodh, Science **309**, 1207 (2005).
[11] S. Gokhale, K. H. Nagamanasa, R. Ganapathy, and A. K. Sood, Soft Matter **9**, 6634 (2013).
[12] M. Rubin-Zuzic, G. E. Morfill, A. V. Ivlev, R. Pompl, B. A. Klumov, W. Bunk, H. M. Thomas, H. Rothermel, O. Havnes, and A. Fouquet, Nat. Phys. **2**, 181 (2006).
[13] H. Löwen, Soft Matter **6**, 3133 (2010).
[14] A. Ivlev, G. Morfill, and H. Löwen, *Complex Plasmas and Colloidal Dispersions: Particle-Resolved Studies of Classical Liquids and Solids* (World Scientific, Singapore, 2012).
[15] D. Rowenhorst and P. Voorhees, Annu. Rev. Mater. Res. **42**, 105 (2012).
[16] R. Evans, Adv. Phys. **28**, 143 (1979).
[17] Y. Singh, Phys. Rep. **207**, 351 (1991).
[18] H. Löwen, Phys. Rep. **237**, 249 (1994).
[19] U. M. B. Marconi and P. Tarazona, J. Chem. Phys. **110**, 8032 (1999).
[20] A. J. Archer and R. Evans, J. Chem. Phys. **121**, 4246 (2004).
[21] P. Español and H. Löwen, J. Chem. Phys. **131**, 244101 (2009).
[22] G. Kahl and H. Löwen, J. Phys.: Condens. Matter **21**, 464101 (2009).
[23] R. Roth, J. Phys.: Condens. Matter **22**, 063102 (2010).
[24] R. Roth, K. Mecke, and M. Oettel, J. Chem. Phys. **136**, 081101 (2012).
[25] K. R. Elder and M. Grant, Phys. Rev. E **70**, 051605 (2004).
[26] H. Emmerich, H. Löwen, R. Wittkowski, T. Gruhn, G. I. Tóth, G. Tegze, and L. Gránásy, Adv. Phys. **61**, 665 (2012).
[27] T. Pusztai, G. Tegze, G. I. Tóth, L. Környei, G. Bansel, Z. Fan, and L. Gránásy, J. Phys.: Condens. Matter **20**, 404205 (2008).
[28] J. Mellenthin, A. Karma, and M. Plapp, Phys. Rev. B **78**, 184110 (2008).
[29] L. Gránásy, G. Tegze, G. I. Tóth, and T. Pusztai, Philos. Mag. **91**, 123 (2011).
[30] S. van Teeffelen, C. N. Likos, and H. Löwen, Phys. Rev. Lett. **100**, 108302 (2008).
[31] T. Neuhaus, M. Schmiedeberg, and H. Löwen, New J. Phys. **15**, 073013 (2013).
[32] B. P. Athreya, N. Goldenfeld, J. A. Dantzig, M. Greenwood, and N. Provatas, Phys. Rev. E **76**, 056706 (2007).
[33] A. Jaatinen, C. V. Achim, K. R. Elder, and T. Ala-Nissila, Phys. Rev. E **80**, 031602 (2009).
[34] S. van Teeffelen, R. Backofen, A. Voigt, and H. Löwen, Phys. Rev. E **79**, 051404 (2009).
[35] K.-A. Wu, A. Adland, and A. Karma, Phys. Rev. E **81**, 061601 (2010).
[36] N. Ofori-Opoku, J. J. Hoyt, and N. Provatas, Phys. Rev. E **86**, 066706 (2012).
[37] K. A. Wu and P. W. Voorhees, Acta Mater. **60**, 407 (2012).
[38] A. Adland, Y. Xu, and A. Karma, Phys. Rev. Lett. **110**, 265504 (2013).
[39] A. Adland, A. Karma, R. Spatschek, D. Buta, and M. Asta, Phys. Rev. B **87**, 024110 (2013).
[40] I. Williams, E. C. Ogŭz, P. Bartlett, H. Löwen, and C. P. Royall, Nat. Commun. **4**, 2555 (2013).
[41] See Supplemental Material at http://link.aps.org/supplemental/10.1103/PhysRevE.88.062316 for movies of the crystal growth.
[42] Y. Rosenfeld, Phys. Rev. Lett. **63**, 980 (1989).
[43] P. Tarazona, J. A. Cuesta, and Y. Martinez-Raton, *Density Functional Theories of Hard Particle Systems* (Springer, Berlin, 2008).
[44] J. F. Lutsko, Adv. Chem. Phys. **144**, 1 (2010).
[45] U. Gasser, E. R. Weeks, A. Schofield, P. N. Pusey, and D. A. Weitz, Science **292**, 258 (2001).
[46] A. Härtel, M. Oettel, R. E. Rozas, S. U. Egelhaaf, J. Horbach, and H. Löwen, Phys. Rev. Lett. **108**, 226101 (2012).
[47] V. Heinonen, A. Mijailović, C. Achim, T. Ala-Nissila, R. E. Rozas, J. Horbach, and H. Löwen, J. Chem. Phys. **138**, 044705 (2013).
[48] T. Biben, R. Ohnesorge, and H. Löwen, Europhys. Lett. **28**, 665 (1994).
[49] R. P. A. Dullens, D. G. A. L. Aarts, and W. K. Kegel, Phys. Rev. Lett. **97**, 228301 (2006).
[50] J. M. Brader, R. Evans, M. Schmidt, and H. Löwen, J. Phys.: Condens. Matter **14**, L1 (2002).
[51] M. Schmidt, H. Löwen, J. M. Brader, and R. Evans, Phys. Rev. Lett. **85**, 1934 (2000).
[52] R. Blaak, S. Auer, D. Frenkel, and H. Löwen, Phys. Rev. Lett. **93**, 068303 (2004).